# PERFORMANCE OF AIR-BREATHING AND ROCKET ENGINES FOR HYPERVELOCITY AIRCRAFT

CHARLES A. LINDLEY

*Senior Staff Engineer, Applied Mechanics Division*
*Aerospace Corporation, El Segundo, California*

## ABSTRACT

Rockets, propellant augmented hypervelocity air-breathers, and aerothermally augmented cycles may be profitably treated as a continuous spectrum of related chemical propulsion devices. On this basis, their performance is developed and correlated in terms of energy and flight velocity. Based upon energy considerations and Reynolds analogy, some limitations on application of aerothermal thrust augmentation are developed.

The performance of a propellant augmented air-breather is shown to be superior to that of the unaugmented air-breather with a separate rocket. Tentative conclusions are drawn regarding the relative merits of various air-breathing and rocket propulsion schemes for several classes of hypervelocity flight missions.

## INTRODUCTION

Over the past five years whole new vistas of air-breathing propulsion potentialities have been opening up at a rate that is somewhat breathtaking to those of us in the field. Some of the new concepts have been discussed before this and other international audiences by Mordell and Swithenbank, Dugger, and others [1–5]. It is now abundantly clear that, in theory at least, the air-breathing powerplant is capable of performing at any desired speed in the atmosphere.

Under these circumstances it must be considered that the air-breathing engine is either presently or potentially a competitor of the rocket for every

atmospheric propulsion task. Propulsion that clearly must occur outside the atmosphere is still the exclusive province of the various types of rockets. The air-breathing powerplants will retain their primacy in the low-speed and low-altitude regimes which they now dominate. But all purely atmospheric propulsion tasks in the hypervelocity-speed regime, and all tasks which could be done on a trajectory either inside or outside the atmosphere, such as orbital boost, must be considered present or future competitive grounds for the rocket and air breather.

To this competition the rocket brings the inherent advantages of simplicity, reliability, low installed engine weight, and present availability. The only clear advantage of the air-breather is a drastically improved fuel specific impulse. Its chief drawback is a low thrust coefficient at extreme velocities, which may lead to large, heavy engine installations such as those sketched in Ref. 3. To minimize this weakness, considerable emphasis here will be placed on various forms of thrust augmentation for the basic air-breathing engine.

We cannot accurately assess the weight penalties of various hypervelocity air-breathing devices at present. We will, however, show certain fundamental performance relationships and limits which will give a partial indication of the powerplant selection appropriate to various missions.

## METHOD OF ANALYSIS

Most of the cycle analysis shown here has been done by a simple, accurate, analytic form of cycle analysis, developed over recent years specifically for use in the hypervelocity regime. The essential features of this analysis are the use of enthalpy and velocity to occupy the central positions held by temperature and Mach number in the older perfect-gas analysis. An energy conversion parameter can then be used to account for real-gas effects. A few essentials of the method are reproduced in Appendix A. Further information is available in Ref. 6.

In consonance with the method of analysis, all assumptions and results are presented in terms of velocity and enthalpy as prime variables, rather than Mach number and temperature. This has many advantages, some of which will become evident.

## MATRIX OF ENGINE VARIABLES

The entire family of chemical rockets and hypervelocity air-breathing engines with fuel-rich, oxidizer addition and aerothermal thrust augmentation may be treated as a continuous spectrum of devices, with varying proportions of fuel, oxidizer and air flow, and varying amounts of aerothermal heat addition. With so many variables involved, a geometric

representation of the continuum with which we will deal may be of considerable help in understanding the results. For this purpose we will construct a three-dimensional framework of the three prime parameters of the study.

First, consider the fuel-air ratio and the oxidizer-air ratio of the air-breathing engine as orthogonal coordinates. This gives us a two-dimensional region as shown in Fig. 1. Along the fuel-air ratio axis lie the stoichiometric and fuel-rich ramjets of all equivalence ratios. We will have little interest in the lean fuel-air ratios at the extreme left. At the extreme right of the coordinate system, the air flow goes to zero. Since the fuel discussed here is liquid hydrogen, we will have to call this limiting case a "cold-liquid" rocket. Its performance is not interesting. With enough heat added to vaporize the hydrogen it becomes a cold-gas rocket, which can have interesting performance for some purposes.

We will ignore points along the second axis. However, we will be interested in those cases along the diagonal line on which the total mixture of fuel, air, and oxidizer is stoichiometric—that is, enough oxidizer is added

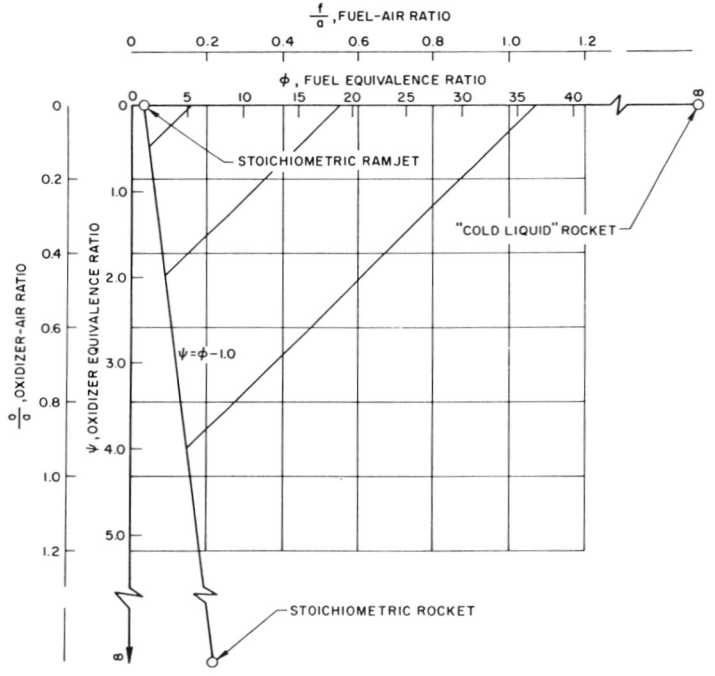


Figure 1. Representation of variables, two-dimensional.

to burn all the excess fuel injected into the engine. This line begins at the stoichiometric ramjet and goes through a series of cases in which excess fuel and oxidizer are added in stoichiometric proportions, ending in the extreme case of the stoichiometric rocket. Thus the conventional ramjet, rocket, and a close kin of the cold-gas rocket all appear in this plane. We will be studying the trends of performance along the lines between them.

The third coordinate of our phase space is the aerothermal energy input, represented by the vertical axis in Fig. 2. The fuel and oxidizer are circulated through the airframe to absorb aerodynamic heating before being injected into the engine. The vertical coordinate is the amount of heat absorbed per pound of propellant. Such aerothermal augmentation adds energy to the propulsive fluids and improves the engine performance. Thus, the region in which we are interested is a prism as shown in Fig. 2, all the upper levels of which are aerothermally augmented cycles.

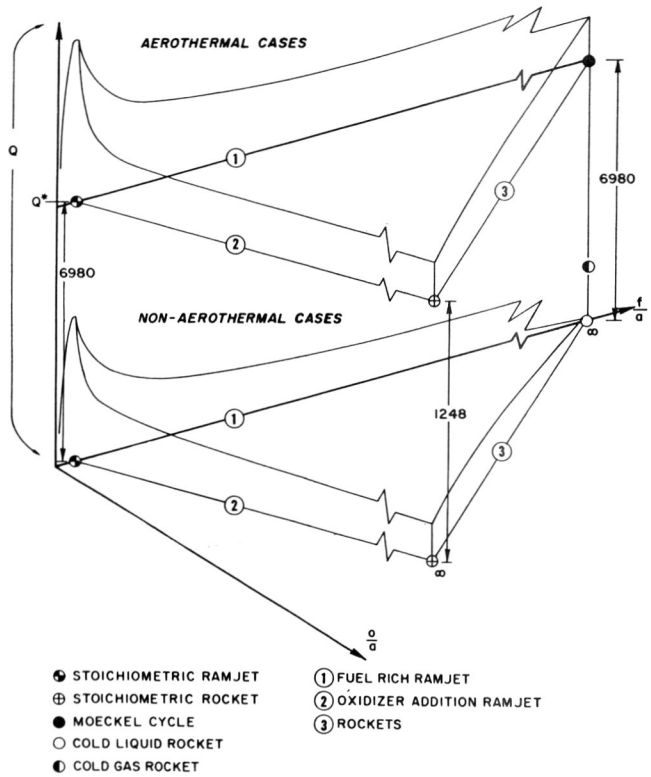


Figure 2. Representation of variables, three-dimensional.

Directly above the cold-liquid rocket is the aerothermal propulsive system first proposed by Moeckel [7] in 1954, which we will refer to as the Moeckel cycle. This is the simplest and most straightforward of all such cycles, in which the coolant fluid is delivered directly to a nozzle and expanded overboard as a hot gas without any chemical reaction. The thermal propulsive energy is obtained entirely from what we will call *aerothermal feedback.*

The corner of the prism above the stoichiometric rocket is an aerothermal rocket, as discussed by Greiner et al. [8] in which the fuel and oxidizer of a rocket are used as coolants. The third upper corner of the prism is the stoichiometric aerothermal ramjet, in which the ramjet fuel is used to regeneratively cool the airframe before being burned by the engine.

It should be clearly understood that the aerothermal-heating term in which we are interested specifically excludes any heat picked up by regenerative cooling of the internal surfaces of the engine, since this heat is extracted from the propulsive stream and merely returned, with no net energy gain. The lines along the top of the prism represent cases directly analogous to the lines below them with the addition of aerothermal augmentation. We will refer to these as the aerothermal fuel-rich ramjet, the aerothermal oxidizer addition ramjet, and the aerothermal rocket.

We will now attempt to explore the behavior of the thrust coefficient and specific impulse along each of the edges of this prism, and along certain additional diagonal cross sections. Of course, we will present these performance curves in standard two-dimensional form. This discussion is intended to clarify relationships between the several variables with which we will deal and to establish the concept of a continuum in which all air-breathing and nonair-breathing chemical engines have a place.

## ENGINE PERFORMANCE

### ROCKETS

The propellant specific impulse for the conventional rocket and related nonair-breathing propulsion devices is given in Fig. 3. These performance curves represent the infinity cross section of the continuum described in Fig. 2. This performance and all performance that follows are for the two propellants, liquid parahydrogen and liquid oxygen, unless otherwise stated. The other significant assumptions are given in Table 1.

In order to clearly understand the discussion that follows on other engines, we must carefully analyze the fundamental relationships that go

**TABLE 1**

*Fuel—Liquid Parahydrogen*

$h_f$ = 51,600 Btu/lb
$h_{0f}$ = −230 Btu/lb
$Q^*$ = 6,980 Btu/lb (at 1980°R)

*Component Efficiencies, etc.*

Diffuser, $\eta_D$ = 0.92
Nozzle, $\eta_n$ = 0.96
Combustion efficiency, 100 percent

No combustor friction losses
Ideally expanded nozzle
Chemical equilibrium nozzle flow

*Oxidizer—Liquid Oxygen*

$h_{00x}$ = 0 Btu/lb
$Q^*$ = 526.9 Btu/lb (at 1980°R)

*Air-Breather Specific*

Flight velocity, $V$ = 20,000 fps
Downstream fuel injection
Propellants preheated to $Q^*$, regeneratively or aerothermally
Oxidizer reacted with fuel before injection
Injection pressure ratio, 27.4
Ambient air enthalpy, $h_0$ = 100 Btu/lb

*Rocket Specific*

Pressure ratio, 4000:1

to make up the lower curve of Fig. 3. Rocket performance at other than stoichiometric fuel-oxidizer ratio can be adequately described by the analytical relationship

$$I = \frac{V_0}{g} = \frac{1}{g}\sqrt{2gJ\eta_n h_f\left[1 - \left(\frac{P_6}{P_4}\right)^{\sigma_n - 1/\sigma_n}\right]} \tag{1}$$

where the propellant heating value $h_f$ is defined for the rich and lean cases by

$$h_f = 5{,}770\left[\frac{1 - f/o}{1 - f/o|_{st}}\right] + h_0 \quad \text{(rich)} \tag{1a}$$

$$= 5{,}770\left[\frac{f/o}{f/o|_{st}}\right] + h_0 \quad \text{(lean)} \tag{1b}$$

and the nozzle-energy conversion parameter, $\sigma_n$, is determined as indicated in Appendix A.

From these relationships, the chemical heat release is described by two straight lines joined at the stoichiometric point shown as the lower curve of Fig. 4. For simplicity we will here set the sensible enthalpy term equal to zero. If there were no variations in the nozzle-energy conversion parameter (defined in Appendix A) with combustion gas composition, the specific-impulse curve would then take the form of the two parabolic curves shown, joined at the stoichiometric line. Maximum rocket performance would occur at the stoichiometric mixture ratio.

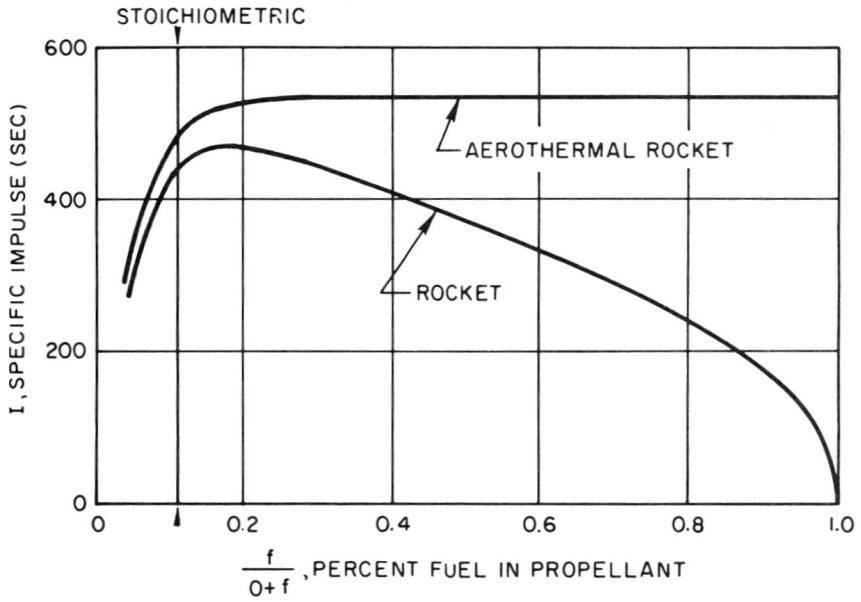


Figure 3. Nonair-breathing engine performance.

The presence of large molar fractions of unburned hydrogen on the fuel-rich side of the curve increases the ratio of specific heats of the gas mixture. This effect causes a rapid increase in the energy-conversion parameter with excess hydrogen, as shown in Fig. 4. This results in a variation of the cycle thermodynamic efficiency term, $\eta_{th}$, as shown, with a strong rise to the right of the stoichiometric line. Obviously, the size of this rise will become less as the pressure ratio decreases.

Inclusion of the thermodynamic efficiency term adds the increment of performance shown in the upper specific impulse curve to give the rocket performance curve its characteristic shape, rising to a smooth peak on the fuel-rich side of stoichiometric despite the fact that the chemical heat release is not maximum there. The peak of the specific impulse curve will shift toward stoichiometric as the pressure ratio $P_6/P_4$ approaches zero.

This type of performance behavior is typical of many previously published results such as those in Ref. 9. Other rationalizations of this effect have been put forward but are not as satisfactory. The present interpretation lends itself to easy extension to the performance peculiarities of the aerothermal rocket and various air-breathing cycles to be discussed later.

*Moeckel Cycle.* For high-cycle pressure ratios such as those assumed in Table 1 for the present computations, the performance of the Moeckel cycle is primarily a function of the amount of aerothermal heat absorbed

by the propellant, as shown in Fig. 5. These performance curves were computed directly from Mollier diagrams for the various propellants shown since, in some cases, they involve two phase flows.

For the sake of certain analytical treatments that follow, an analytic representation of the Moeckel cycle performance is required. For this purpose we will use the expression of Eq. (1) where the chemical heating value is zero and only the sensible heat of the propellant remains:

$$h_f = h_{of} \cong Q \tag{2}$$

For the large pressure ratios which we are examining, the effect of the pressure ratio and energy conversion parameter on the energy conversion efficiency may be adequately represented by a constant Moeckel cycle energy conversion efficiency. This leads to the analytical formulation

$$I = \frac{1}{g}\sqrt{2gJ\eta_R Q} \tag{3}$$

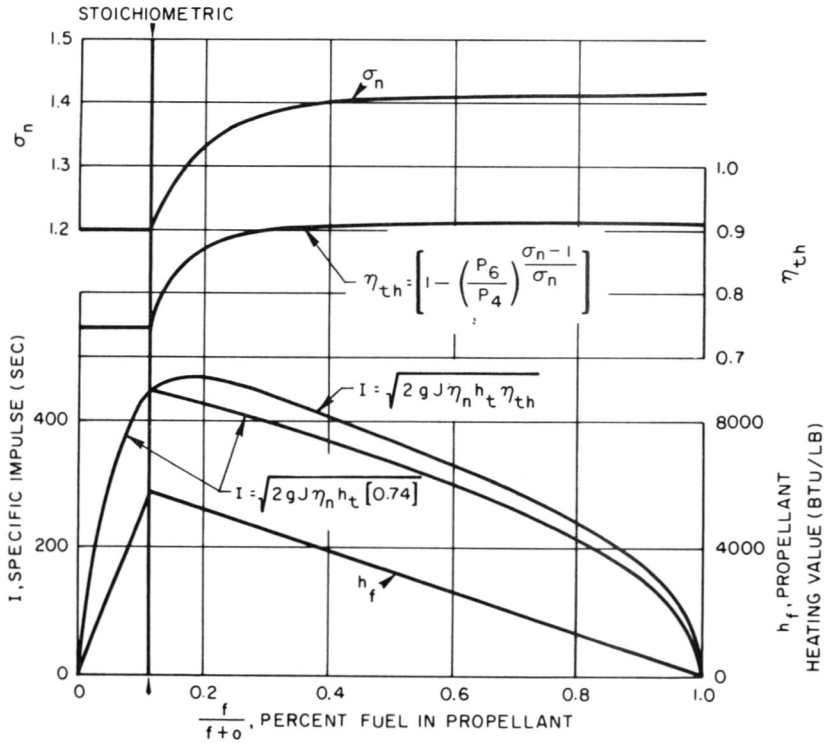


Figure 4. Basic parameters in rocket performance.

This relationship for conversion efficiencies of 0.80 and 1.00 is represented by the dashed curves in Fig. 5. The correlation is excellent for helium and hydrogen. The correlation is much poorer for water because its heat of vaporization is large compared to the total heat absorbed at allowable engineering temperatures.

For later analyses we will assume that the performance of the Moeckel cycle is adequately represented by the curve of 80 percent conversion efficiency. The curve will be considered universal for all coolants except that the coolant enthalpy limit varies greatly with the coolant. The higher molecular weight coolants have a much lower coolant enthalpy limit.

*Aerothermal Rockets.* We have discussed the lower curve of Fig. 3, giving rocket performance for varying stoichiometries, and located the right end point of the upper curve, which is the value of the Moeckel cycle specific impulse for hydrogen propellant at the conditions of Table 1.

The specific impulse of the aerothermal rocket for other mixture ratios of fuel and oxidizer is shown by the remainder of the upper curve of Fig. 3. It is assumed that both fuel and oxidizer have absorbed aerothermal heat

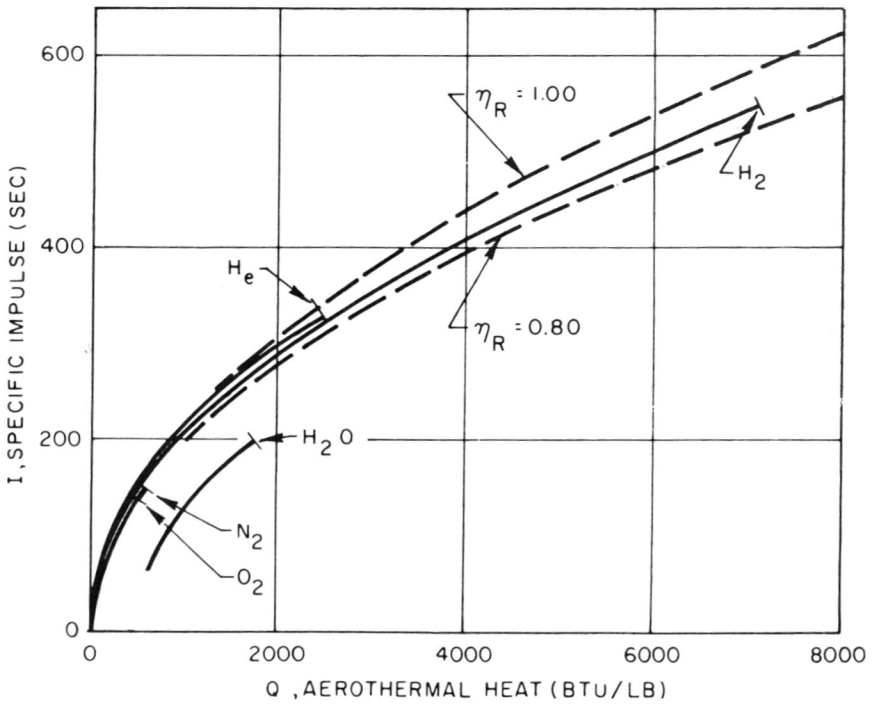


Figure 5. Moeckel cycle performance.

to the maximum allowable temperature. Because of the great heat content of the hydrogen, the total of combustion and aerothermal heat is practically constant from stoichiometric mixture ratio to pure fuel. Therefore the variation of specific impulse near the stoichiometric mixture is caused almost entirely by the variation of gas properties as discussed in the rocket case. The excess hydrogen in the fuel-rich combustion products causes an increase of the energy conversion efficiency.

The curve is practically constant from 30 percent to 100 percent fuel, reflecting the nearly constant enthalpy and conversion efficiency. Thus the aerothermal rocket gives us practically constant specific impulse over a very broad variation of propellant-mixture ratios provided an adequate amount of aerothermal heating is available. This property of the aerothermal rocket will be explored further.

## AIR-BREATHING ENGINES

The ideal thrust coefficient of a fuel-rich air-breathing engine is given by

$$C_{Fi} = \frac{f}{a}\left[\frac{2gJh_f^*}{V} + 1\right] \tag{4}$$

where

$$h_f^* = h_f;\ \phi \leqslant 1$$

$$= h_f/\phi;\ \phi \geqslant 1$$

as shown in the two straight lines forming the upper dashed curve of Fig. 6 for the conditions of Table 1. This assumes that the sum of the chemical and kinetic energy of the fuel is completely converted to thrust work for lean-mixture ratios. For fuel-rich operation, stoichiometry forbids conversion of additional chemical energy and only the kinetic energy of the excess fuel appears.

The corresponding ideal specific impulse is given by

$$I_i = \left[\frac{Jh_f^*}{V} + \frac{V}{2g}\right] \tag{5}$$

shown by the upper solid curve of Fig. 6. For lean operation, the ideal specific impulse is constant at 2318 sec. For extremely high equivalence ratios, it approaches the kinetic energy value of 311 sec as a limit. This and all following air-breathing engine performance curves are at a flight speed of 20,000 fps.

The performance of the subsonic burning ramjet over this range of equivalence ratios as developed from Eq. (1A) of Appendix A is shown by the lower curves of Fig. 6. The ideal-thrust coefficient is reduced by approximately the sum of the inlet and exit flow processing loss terms, or about 0.12 at all equivalence ratios. Thus, the effect of inlet and nozzle losses on hypervelocity air-breathing engine performance can almost be treated as a constant-drag coefficient decrement from the ideal-thrust coefficient over a broad range of equivalence ratios. The variation of this thrust-coefficient decrement at equivalence ratios near unity is very significant, since the ideal impulse in this region is very high and the actual impulse is reduced to zero, as seen in the figure. The rapid change in the thrust-coefficient decrement between equivalence ratios of one and four is another manifestation of the rapid increase of the nozzle-energy conversion

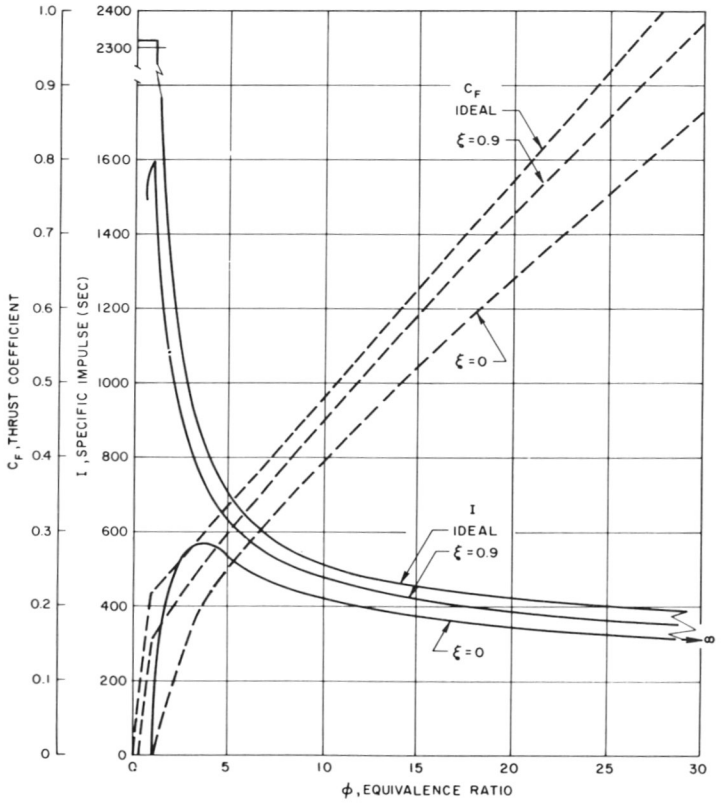


Figure 6. Air-breathing engine performance.

parameters of the exhaust gases with increasing amounts of excess hydrogen, as previously described in the rocket cases.

Since the ideal thermodynamic cycle losses for the subsonic combustion ramjet are negligible at this velocity and the flow processing losses make up most of the performance loss, the most effective way to obtain increased performance is to change to the supersonic combustion ramjet cycle to reduce the flow processing losses. This change also drastically reduces the engine internal pressure containment and local heat transfer rate problems, as has been pointed out in Refs. 1 and 2.

Let us now look at the performance for diffusion of only 10 percent of the inlet kinetic energy ($\xi = 0.9$). If we assume that the inlet and exit losses are proportional to the diffuser kinetic energy reduction [Eqs. (12A) and (13A), Appendix A], the flow processing losses will be one tenth of the subsonic combustion ramjet losses. The thermodynamic cycle loss increases slightly, but the performance moves sharply toward the ideal, especially at low equivalence ratios, as shown by the middle curves in Fig. 6. This allows us to obtain most of the theoretical performance at an equivalence ratio of one. Thus, supersonic combustion gives us the option of obtaining extremely high impulses if the corresponding low values of thrust coefficient are acceptable.

The manner in which impulse varies with the amount of diffusion done under the present inlet and nozzle loss assumption is shown in Fig. 7. Note that the slope of the impulse curves is nearly linear for $0 < \xi < 0.6$. This portion of the curves is well described by the first-order terms of the perturbation analysis of Eq. (16A) in the Appendix, from which

$$I = \frac{V}{2g}\left(C_0 + D_0\right)\frac{\xi}{f/a} + \text{const.} \tag{6}$$

However, nonlinear, higher-order terms representing the thermodynamic cycle losses take over abruptly as $\xi \to 1$.

At the limit of no diffusion, all the impulse curves converge to the same point, which is the impulse corresponding to the velocity of the fuel injection. This point is not physically meaningful because it assumes a duct with no diffusion and absolutely no losses, which cannot be attained. All equivalence ratios with higher specific impulse than this value show maxima, while all equivalence ratios with specific impulse below this value show a rise in the nonlinear region and therefore have no maxima.

Where an optimum exists, the optimum value of $\xi$ increases with increasing flight velocity. It is, however, almost independent of all other parameters, and therefore is rather easy to locate numerically. It can be

located analytically by differentiation of Eq. (15A) of Appendix A, but the resulting expression is so complex that it takes longer to evaluate it numerically than to locate the optimum by iteration. In what follows the value of $\xi$ for maximum performance was always located by iteration where a maximum exists.

*Fuel-Rich Ramjet.* The thrust coefficient and specific impulse of the fuel-rich supersonic combustion ramjet with and without aerothermal augmentation at the conditions of Table 1 is shown in Fig. 8 along with the corresponding ideal-thrust coefficients. The thrust-coefficient curves closely parallel the ideal performance. Aerothermal augmentation adds very little energy and therefore very little thrust at an equivalence ratio of one, but the energy addition is proportional to the fuel-air ratio, and rises to very substantial values for large equivalence ratios, where the specific impulse is nearly doubled. The lowest specific impulse curve in the figure will be discussed in a later section.

The aerothermally augmented cycle can give impulses in the 600-700-sec range over a broad range of large thrust coefficients. Since large thrust coefficients mean that a small inlet may give adequate thrust, an engine of

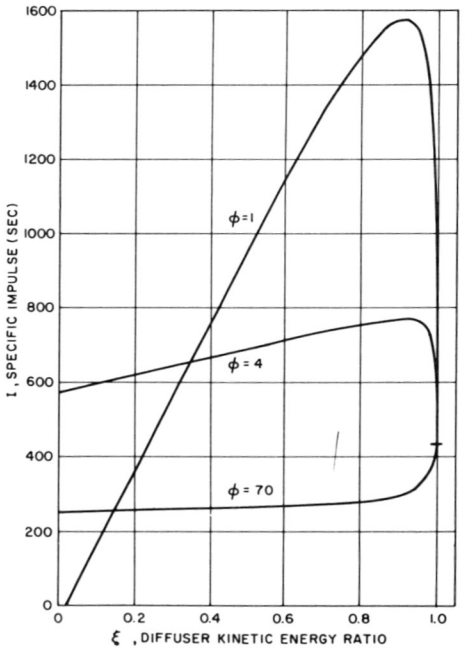


Figure 7. Performance variation with degree of diffusion.

this sort may find useful application. It must be remembered, however, that to get the impulse shown it is necessary to obtain the large amount of aerothermal energy required to heat the fuel. This and other energy considerations of the application of this cycle will be discussed in the next section.

*Oxidizer Addition Ramjet.* The performance of the oxidizer addition ramjet and its aerothermal counterpart is shown in Fig. 9. Because all the chemical energy of the fuel is released, the thrust augmentation by oxidizer addition with modest equivalence ratios is very high. The thrust coefficient of the basic cycle approaches two for an equivalence ratio of only five. This corresponds to a total propellant consumption approximately equal to the air flow. Under this circumstance the air becomes only a small oxidizer augmentation of the total flow and the engine could be regarded as a hot-air supercharged rocket. The performance varies accordingly, with high

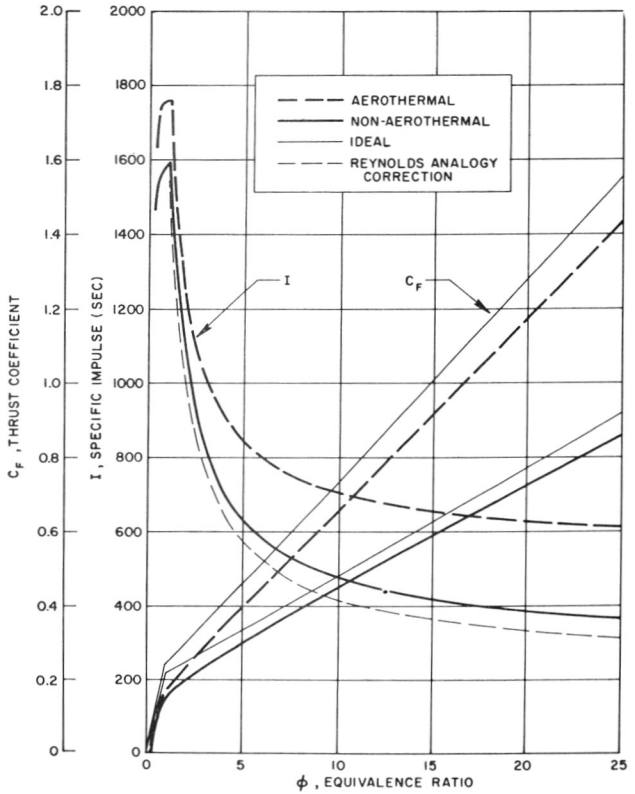


Figure 8. Fuel rich air-breathing performance.

values of specific impulse for equivalence ratios near unity, but with propellant specific impulse approaching that of the rocket for the higher equivalence ratios. The ideal-thrust-coefficient curves are again shown for comparison, and the cycle energy conversion efficiency is obviously high.

The aerothermal augmentation of this cycle can be seen to contribute very little to its total performance. The cycle does not consume enough hydrogen to carry very much heat. The oxidizer is also assumed to carry aerothermal heat, but its total heat content is so low that most of the aerothermal augmentation shown could have been obtained by heating only the fuel.

*Comparison of Types of Augmentation.* From the propulsion point of view, fuel-rich augmentation, oxidizer addition, and aerothermal augmentation are all means of obtaining a substantially increased thrust coefficient of the air-breathing engine at various costs in the resulting specific impulse.

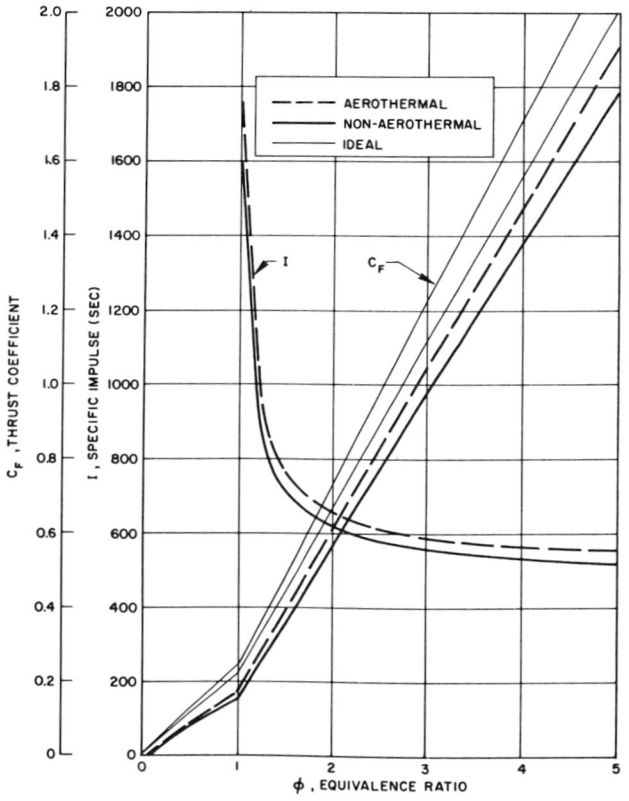


Figure 9. Oxidizer addition air-breathing performance.

Figure 10 compares the effectiveness of these different means of thrust augmentation. Curves of specific impulse versus thrust coefficient are given for fuel-rich and oxidizer addition augmentation, with and without aerothermal augmentation.

At a flight speed of 20,000 fps, the stoichiometric ramjet has a thrust coefficient of approximately 0.149 and a specific impulse of approximately 1590 sec under the present assumptions. The only means of augmenting this thrust coefficient and simultaneously increasing the specific impulse is aerothermal augmentation. This gives an increase in both thrust and specific impulse of about 10 percent. Because of the interrelation of impulse and thrust coefficient for the air-breather, both of these points lie on a straight line passing through the origin of coordinates, as do all other points with identical propellant-to-air ratios.

Thrust augmentation by addition of excess fuel causes the impulse to fall off as shown by the lower curve. This curve passes to specific impulses

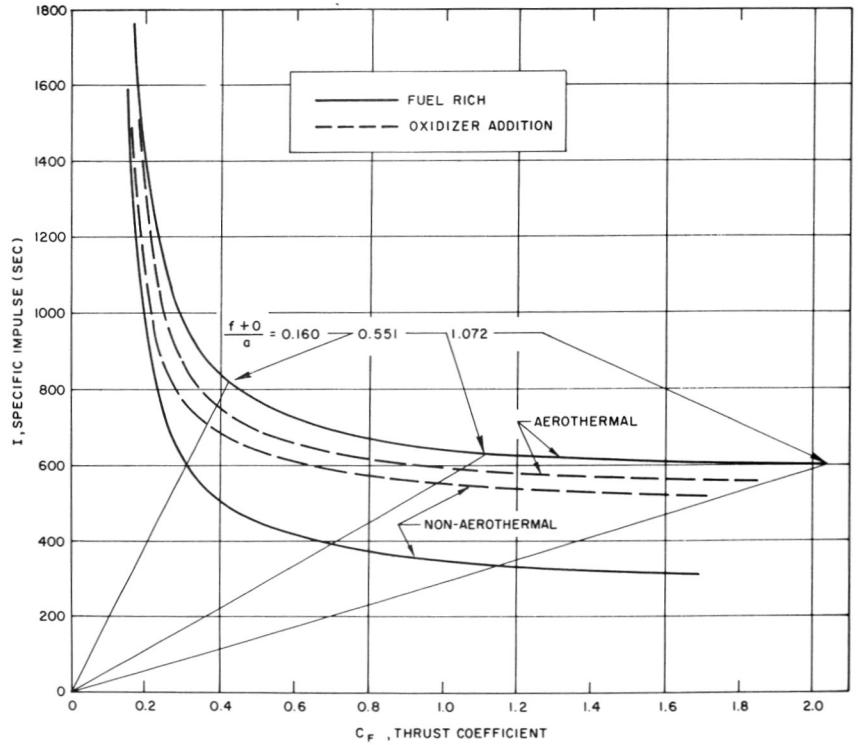


Figure 10. Comparison of thrust augmentation effectiveness.

below 600 sec for about double the unaugmented thrust. The next higher curve is the performance with stoichiometric oxidizer addition. This technique can quadruple the thrust before the specific impulse drops to 600 sec, and the performance always exceeds that of a rocket. The combination of aerothermal augmentation with oxidizer addition is only slightly better, as shown. The upper curve of the figure shows the performance attained with maximum aerothermal augmentation of the fuel-rich engine. The specific impulse does not fall below 600 sec until the thrust has increased by more than ten times. However, this performance is possible only if an extremely large amount of aerothermal heat is available. The restrictions that this requirement implies are examined in the following sections.

Since the peak performance for a rocket occurs at a propellant mixture slightly richer than stoichiometric, we might expect the same effect in the propellant augmented air-breathing portion of the propulsion continuum. To confirm this, Fig. 11 shows the specific impulse variation for the diagonal constant propellant fraction lines indicated in Figs. 1 and 10. The left ends of the curves are cut off at the overall stoichiometric values. The curves for no aerothermal augmentation show the same peaking for slightly fuel-rich overall mixtures that the rocket shows, except that the effect fades away for the lowest propellant increment shown. The results with aerothermal augmentation show a similar family relationship to the aerothermal rocket.

The overall efficiency $\eta_\Sigma$ of conversion to thrust work of the total chemical and kinetic energy of the fuel is shown in Fig. 12 for the fuel-rich and

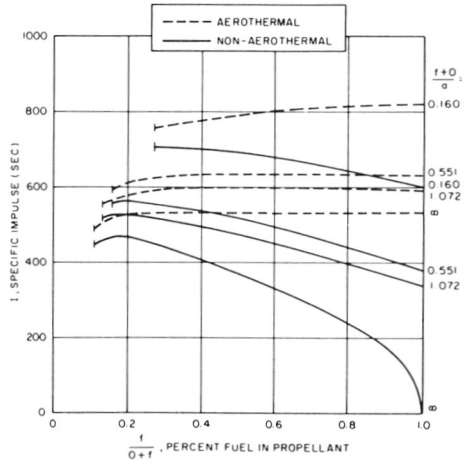


Figure 11. Sectional contours of the performance matrix.

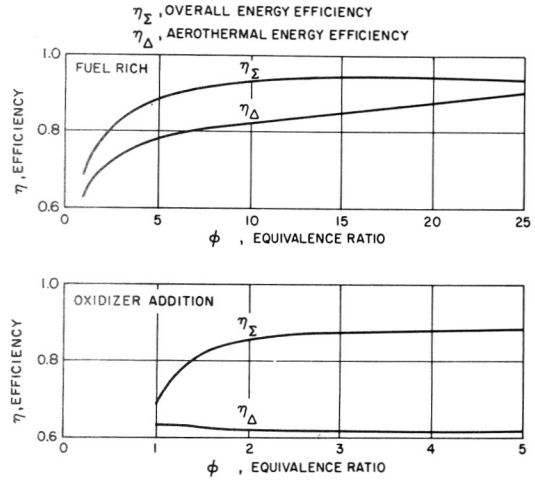


Figure 12. Energy conversion efficiencies of the air-breathers.

oxidizer addition ramjets. The efficiency $\eta_\Delta$ of conversion of the aerothermal energy into an increment of thrust-work is also shown. This aerothermal energy conversion efficiency will be discussed again.

## COOLING LIMITATIONS ON AEROTHERMAL PROPULSION

We have analyzed the aerothermal propulsion devices as though aerodynamic heat were available in unlimited quantities. We have recognized only that there is a limit on the amount of heat that can be absorbed per pound of coolant fluid. This corresponds to the difference between the fluid enthalpy in the condition in which it is stored, usually a liquid, and the enthalpy at the maximum allowable coolant temperature, a little lower than the allowable working temperature of the heat-exchanger materials. A second limitation on the aerothermal heat energy available for propulsion augmentation arises from conservation of energy and the application of Reynolds analogy as developed in Ref. 10.

The rate at which energy is dissipated by the aerodynamic drag of the vehicle is

$$DV = \text{drag energy rate} \tag{7}$$

Of this energy, only the frictional drag fraction, which we will define as

$$\nu = \frac{D_f}{D} \tag{8}$$

is actually dissipated in the boundary layer adjacent to the vehicle. Only a fraction $R$ of the heat so generated in the boundary layer is actually absorbed by the body. $R$ may take on values from zero up to approximately one half, where the Prandtl number is one and the wall is cold.

$$0 < R < R^*; \qquad R^* \cong \frac{1}{2} \tag{9}$$

The value of $R$ will usually be close to $R^*$ in the hypervelocity regime because practical aircraft materials cannot tolerate temperatures that are appreciable compared to the recovery temperature. This conclusion would be modified if an appreciable fraction of the surface heating were removed by radiation, but the fourth-power relationship keeps the amount of radiation small if the surface temperature is significantly below the radiation equilibrium value. The aerothermal heating rate is thus defined as

$$\dot{w}QJ = \nu RDV \tag{10}$$

The primary methods available for increasing the frictional drag fraction are the use of slender bodies and wings, and flight at low angles of attack. Under these circumstances the frictional drag fraction can be pushed to perhaps 0.6 with reasonable engineering configurations.

## PERFORMANCE LIMITS OF MOECKEL CYCLE

We will now examine the performance and thrust limits for the Moeckel cycle, using the simplified analytical representation of Eq. (3). From this and the relation between aerothermal heating and drag of Eq. (10), we obtain the relation between impulse and thrust-drag ratio

$$\omega = \frac{2V}{g}\left(\frac{\nu R \eta_r}{I}\right) \tag{11}$$

This relationship is shown for a specific case in the lowest curve of Fig. 13. The value of the parameter, $\nu R \eta_r$, is representative of a very clean aerodynamic configuration, which leads to the maximum values of the thrust-drag ratio. The maximum impulse of the Moeckel cycle for hydrogen coolant occurs at a vehicle thrust-drag ratio of only 0.6. Thrust greater than the drag can be obtained with excess hydrogen coolant flows, but only at the expense of a drastic reduction of propellant specific impulse as indicated by the curve. Approximate cutoff values corresponding to maximum allowable temperatures of other coolants are indicated on the curve.

Thus to the extent that the analytic curve proposed in Fig. 5 can represent Moeckel cycle performance for all coolants, the relationship between thrust level and impulse is represented by a single line in Fig. 13 with different cutoff values for different coolants. Impulses competitive with the conventional rocket can be obtained only with hydrogen or helium coolant and at thrust-drag ratios of less than one. Other coolants are excluded from the high-impulse, low-thrust region.

## OXIDIZER ADDITION AUGMENTATION OF THE MOECKEL CYCLE

A more efficient means of augmenting the thrust of the Moeckel cycle where thrust-drag ratios greater than 0.6 are required is to maintain the minimum required fuel flow and add oxidizer as necessary to obtain the required thrust. The performance given in the upper curve of Fig. 3 leads to the lowest light curve of Fig. 13. Thus, the specific impulse of the cycle may be maintained at approximately a constant level while satisfying the coolant requirements and increasing the thrust level by more than five times.

The performance shown assumes that the oxidizer is also fully utilized as coolant. Impulses fall slightly at the higher thrust levels if only the fuel is aerothermally heated.

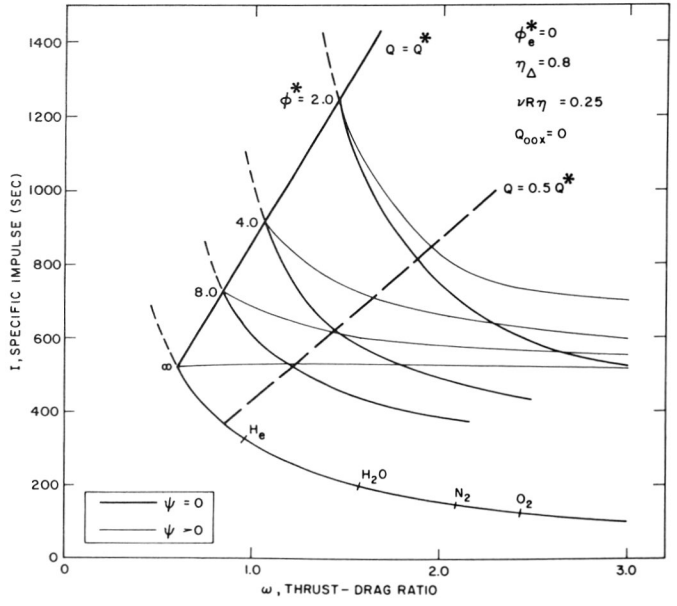


Figure 13. Aerothermal performance limits.

A significant disadvantage of such a system is that the desired ratio of propellants at takeoff cannot be predicted for applications where the thrust schedule cannot be predicted in advance. The method also requires considerable flexibility in the metering and control system of the engine. Nevertheless, the increased performance and flexibility must surely make it considerably more attractive than the pure Moeckel cycle for applications such as the synergetic plane change in which thrust-drag ratios of one or greater are required and flexibility of thrust programing may be of significant benefit.

## PERFORMANCE LIMITATIONS OF AEROTHERMAL RAMJETS

We will now develop the same sort of performance and thrust level relations for the case of the aerothermal ramjets. Since we have an additional parameter at work, the sizing of the engine and resultant airflow, the relations will be a little more complex in this case.

At this point we make use of the aerothermal energy conversion efficiency for the fuel-rich case shown in Fig. 12 and defined in terms of the aerothermal specific impulse increment by

$$\Delta I_a = \eta_\Delta \left( \frac{Q_v J}{V} \right) \tag{12}$$

We specify the vehicular component of aerothermal heating to emphasize the fact that in the air-breathing aerothermal engine a significant amount of fuel cooling capacity may be used for internal regenerative cooling of the engine itself. Since energy obtained from this source does not represent a net profit to the cycle, it must be subtracted from the enthalpy balance. Making these adjustments, the impulse of the aerothermal air-breathing cycle becomes

$$I = I_0(\phi) + \frac{\eta_\Delta J Q_v}{V} \tag{13}$$

For the accuracy required here, we will assume that the efficiency curves of Fig. 12 are adequately represented by the constant, $\eta_\Delta = 0.80$.

The aerothermal energy conversion efficiency usually has a value less than unity, and is treated here loosely as an "efficiency." However, because of the highly nonlinear interaction of the aerothermal energy with the other input energies of the cycle, aerothermal augmentation can sometimes result in the conversion of more thrust work than the aerothermal energy input. The awkward situation of a conversion efficiency greater than unity (and highly variable) would occur here for the Moeckel cycle

and the aerothermal rocket. For this reason we defined and used a different and more constant conversion efficiency in Eqs. (3) and (11) for the Moeckel cycle case.

If we now go through the same procedure as we did for the Moeckel cycle, we obtain

$$\omega = \nu R \eta_\Delta \frac{V I_0}{\eta_\Delta J Q_v} \tag{14}$$

The term $\nu R \eta_\Delta$ in this equation is a nondimensional group of fundamental significance which will appear repeatedly in this discussion. Physically, it is the fraction of the aerodynamic drag that can be recovered as aerothermal heat and converted into thrust. We will refer to it as the aerothermal feedback. A similar group appears in the Moeckel cycle case, but because of a different efficiency definition, it must be multiplied by a propulsion efficiency to be equivalent.

We must still interrelate the engine cooling load, the vehicle cooling load, the engine-coolant flow, and the engine airflow. We will here assume that the critical coolant load of engine and vehicle requires a fuel flow resulting in a critical equivalence ratio of $\phi^*$ with the engine airflow. Of this, an equivalence ratio of $\phi_e^*$ is required to cool the engine, which has the same limiting fuel temperature. The resulting relation is

$$Q_v = Q^* \left[ \frac{\phi^* - \phi_e^*}{\phi} \right] \tag{15}$$

The resulting relations between specific impulse and thrust-drag ratio for a large value of aerothermal feedback, for no engine cooling load, and for various values of the critical equivalence ratio are given by the curves for $\psi = 0$ in Fig. 13. The Moeckel cycle curve is included as $\phi^* = \infty$. The progression of the curves is simple and logical. For any given coolant enthalpy ($Q$) level, the thrust-drag ratio and the impulse increase steadily with increasing airflow (decreasing $\phi^*$) as more fuel receives air for combustion. At the same time, the curves have the same basic character as the Moeckel cycle, with maximum specific impulse and minimum thrust at the coolant temperature limit, and decreasing performance for higher thrust levels. The curves would not be identical for different coolant fuels, however, because of the varying combustion constants of different fuels.

As with the Moeckel cycle, thrust augmentation above the minimum required coolant flow can be obtained more economically by oxidizer addition than by excess fuel flow. Performance for increasing oxidizer flow with constant fuel flow is shown by the light lines. In this case, no heat absorption by the oxidizer is assumed.

The effects of parameter changes for the fuel-rich cases are shown in Fig. 14. The performance map for an engine with a cooling requirement of one equivalence ratio ($\phi_e^* = 1.0$) is shown by the heavy lines, with the basic map of Fig. 13 shown in light lines for comparison. The difference is significant only for small critical equivalence ratios (large airflows), where the specific impulse is slightly lower because of decreased aerothermal augmentation, and the thrust level is much higher because a larger engine is required for a given net airframe cooling capacity.

The very compressed performance map at the left of Fig. 14 shows how the basic map changes when the aerothermal feedback becomes very small, as it does for high-angle-of-attack flight and relatively blunt lifting bodies. The value of the aerothermal feedback chosen is representative of a body like the NASA M-2 shape at a high angle of attack. The specific impulse level remains the same, but the thrust level scales down in proportion to the aerothermal feedback. Large thrust levels can be obtained only at the lower specific impulses. A decrease in flight velocity has the same effect.

## INTERNAL COOLING LIMITS

We should note in passing that an analogous set of aerothermal energy limits occur within the engine. For the air-breathing engines without aerothermal augmentation, we have assumed that the propellants are injected

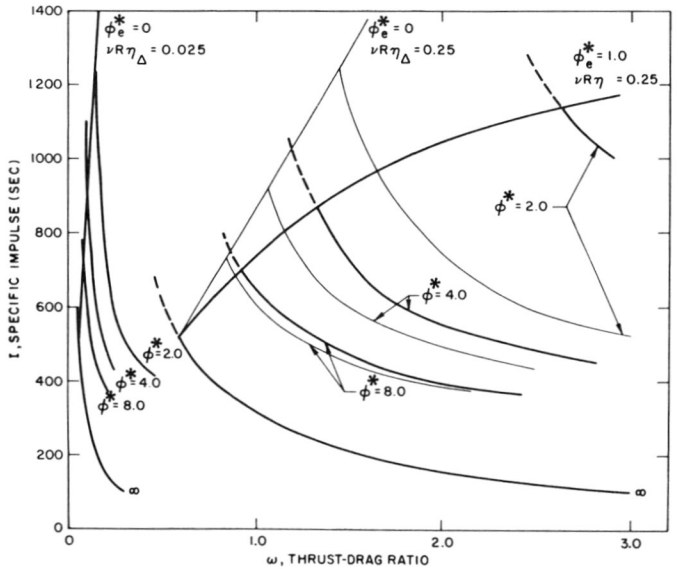


Figure 14. Aerothermal performance limits.

downstream at a velocity corresponding to a limiting coolant temperature expanded through a given pressure ratio, as listed in Table 1. The heat is assumed to come from internal engine regenerative cooling, so there is no net addition of enthalpy to the cycle.

Reynolds analogy forbids heat transfer on the inside of the engine in excess of half the internal viscous energy dissipation. Of course, the velocity and total enthalpies vary through the cycle. To account for this, we pick the maximizing values of each parameter. The resulting expression is

$$Q \leqslant \frac{(C_0 + D_0)(1 - \xi)\, R^*}{f/a} \left[ \frac{V^2}{2gJ} + h_f \right] \tag{16}$$

More enthalpy than this cannot be extracted from the cycle at the given speed and heat addition with the flow losses assumed.

This limit was violated in the performance computations of the previous sections, and they provide a good test case to determine its significance. It affects only the cases without aerothermal augmentation, and the effect is through reduction of the fuel injection velocity. In the nonaerothermal oxidizer addition case, chemical reaction of the injectants supplies the necessary energy, and the injection velocity does not change significantly. In the fuel-rich case the available regenerative heat is so small that the fuel injection velocity becomes negligible for equivalence ratios above five. The resulting reduction of engine specific impulse is shown by the lower dashed curve of Fig. 8. Fortunately, the performance correction becomes significant only for cases where the nonaerothermal fuel-rich performance is very uninteresting in any case.

## MISSION CLASSIFICATION AND PREFERRED PROPULSION

We will now examine the relative merits of these propulsion systems in certain idealized missions. Our discussion must necessarily be very superficial because the potential missions are not well understood and the weights of the propulsive systems and airframes are necessarily quite speculative. It must also be remembered that our treatment neglects several significant real-engine effects, notably possible underexpansion and frozen flow in the nozzle. Nevertheless, a few worthwhile points can be made.

### EFFECT OF AUGMENTATION ON TOTAL PROPULSIVE WEIGHT

Lacking more definitive knowledge, we will assume that the combustor and exit of a hypervelocity air-breather weighs as much as a rocket of the

same thrust, and the weight of an inlet bears the same proportionality to its captured stream thrust. This leads to the simple relation

$$\frac{W_e}{T} = k\left(\frac{C_F + 4}{C_F}\right) \tag{17}$$

where $k$ is the weight-thrust ratio of a rocket. This formulation gives us a smooth transition from rocket to air-breathing engine weights with a reasonable functional relationship. It also states that an air-breathing engine with thrust augmentation has exactly the same weight as an unaugmented air-breather of the same capture area plus a rocket large enough to make up the same total thrust, which seems conservative.

If we represent the mission propulsive effort by an equivalent velocity increment, $\Delta V$, and ignore variations of specific impulse with velocity, the total propellant and power plant fraction becomes

$$\frac{W_p}{W_0} = 1 - e^{[-(\Delta V/I_0)]} + \frac{T}{W_0}\left(\frac{W_e}{T}\right) \tag{18}$$

Based on these two expressions and the nonaerothermal oxidizer addition performance of Fig. 10, we can obtain the solid curves of Fig. 15 as representative of the variation of total propulsive fraction with velocity increment and augmented thrust coefficient for the nonaerothermal oxidizer addition ramjet for a constant thrust mission. The aerothermal rocket and Moeckel cycle are represented by a single set of points in the figure. The figure suggests that the nonair-breathing engines are superior for the lower equivalent velocity increments, while the air-breather with no propellant augmentation is superior for the higher increments. The exact value of the breakeven velocity increment is conjectural because of the speculative nature of the air-breathing engine weight estimate. But the general character of the curves and their trend with varying degrees of augmentation are of a more fundamental nature.

The lack of an optimum for intermediate thrust coefficients suggests that propellant augmentation may not be profitable as a prime mode of operation. However, the curves also suggest that it can be a means of obtaining flexibility of operation at very little performance penalty. Propellant augmentation can be used for thrust-level excursions for maneuvering and glide energy management in the air-breathing system. It may also be useful to eliminate the need for engine variable geometry, or to extend the operating range, as at high speed, without increasing the inlet size.

It might logically be asked how the combination of a rocket plus an unaugmented air-breather would compare with the augmented air-breather.

The dashed curves in Fig. 15 show this case. Since the assumed engine weight is identical, the figure shows only the effect of a slight reduction of the combined impulse of separate engines compared to a single augmented engine. Therefore, the separate engines must be lighter in total weight or show some operational advantage to be chosen over the augmented air-breather for flexibility of thrust level.

The location of the points representing the aerothermal rocket and Moeckel cycle in Fig. 15 suggests that aerothermal rocket augmentation may always be profitable. If, as suggested by Dukes [11], the weight of a convectively cooled airframe, including the coolant, plumbing, and pumps, may be no more than the weight of an ablation- or radiation-cooled airframe, then the overall performance of an aerothermal augmentation system is even better than this formulation would suggest. However, the aerothermal component of the thrust is always limited by the considerations of the last section.

## REPRESENTATIVE MISSIONS

Let us now consider various representative missions and determine what judgments we can make at this early date as to the likely powerplant choices.

*Glide Extension.* As recoverable spacecraft and recoverable boosters lead to lifting reentry, the problem of cross-range extension to reach

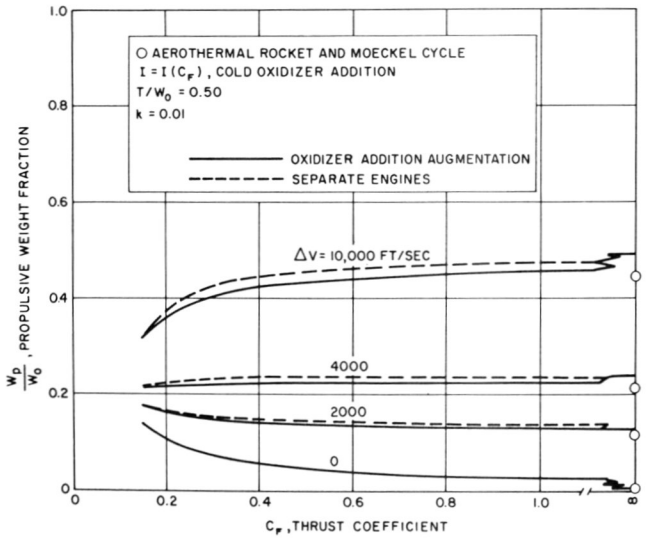


Figure 15. Effect of power plant and velocity increment on total propulsive fraction.

desired landing points will receive greater attention. While cross-range extension can be obtained by increased lift-drag ratio at the cost of significant structural weight, we should not overlook the alternative possibility of gaining cross-range by direct propulsion. Of particular interest are the aerothermal propulsion schemes to cool the airframe during reentry.

The required velocity increment for significant glide extension is not large, perhaps 5,000 fps. The required thrust level is very low, probably less than the drag.

The Moeckel cycle appears to be most attractive for this mission, perhaps with moderate oxidizer augmentation. Provision for thrust reversal might be very effective for increasing the ability to adjust the landing site if the coolant flow cannot be shut off. If orbital retrothrust is required, the engine could probably be converted to a pure rocket very easily.

*Cruise.* Another typical class of missions is represented by cruise at constant speed in the atmosphere. The thrust-drag ratio is unity, and higher thrust for acceleration is normally needed only in the initial acceleration, where the cruise air-breather would usually have a thrust margin. The installed thrust requirement is considerably smaller than that assumed in Fig. 15, so the air-breathers excel for very moderate velocity increments. The stoichiometric air-breather has a clear advantage for practically all cases. Aerothermal augmentation is profitable if it costs practically no airframe weight and if the engine requires less than stoichiometric flow for cooling.

*Synergetic Plane Change.* Certain space maneuvers between low earth orbits, such as orbital plane change and phase change, can be accomplished more efficiently by aerodynamic use of the upper atmosphere than by direct space propulsion. The velocity lost to atmospheric drag must be regained by some propulsive device to return to orbit.

This maneuver is representative of a large class of related missions. Space propulsion is needed, which demands a rocket. Large variations in thrust level are required. The required velocity increment is generally in the middle range of the values shown in Fig. 15.

The cooling problem is severe because the vehicle should plunge into the atmosphere far below the equilibrium glide corridor. This suggests aerothermal propulsion schemes, which would lead to large thrust while in the atmosphere. However, the dynamically preferred thrust schedule is to allow the velocity to decrease during the atmospheric traverse and to accelerate back to nearly orbital speed upon leaving the atmosphere. The severe aerodynamic heating also makes the design of an air-breather difficult.

The choice of powerplant for such missions cannot be made without more detailed information. The rocket will probably be the best choice, with

aerothermal augmentation worth considering. The effect of active cooling on airframe weight will be a critical factor in the decision.

*Boost.* The last type of typical hypervelocity mission we will consider is the boost mission. Usually this is a portion of the acceleration from zero speed at sea level to orbital velocity at an altitude outside the atmosphere. Of the missions discussed, this one can most clearly be performed either inside or outside the atmosphere.

The required thrust level of the air-breather may be higher than that assumed in Fig. 15, and the air-breather may also require more airframe weight in heat protection than the competitive rocket vehicle. Therefore the velocity increment for which our formulation gives the air-breather the advantage would shift to an even higher value.

On the other hand, the velocity increment required by the mission is extremely high. Also, this case is the most sensitive to the validity of the crude assumptions we made for the engine weight and to the omission of the variation of specific impulse with velocity. Therefore we must consider the present analysis entirely inadequate to judge the boost case and await more definitive weight estimates.

## CONCLUSIONS

1. Many of the characteristics of hypervelocity chemical propulsion systems can be adequately analyzed and correlated on a simple velocity and energy basis.
2. Rockets, propellant augmented air-breathers, and aerothermally augmented cycles may be treated profitably as a continuous spectrum of related chemical propulsion systems.
3. In an air-breathing engine at high flight speeds, the loss of available kinetic energy of the captured airflow in the inlet and nozzle may exceed the chemical heat addition. Good performance may be regained if the flow processing losses can be reduced substantially by resorting to supersonic combustion.
4. If the flow processing losses are kept small, the performance can closely approach ideal energy conversion at any speed in the hypervelocity range.
5. Fundamental energy limits restrict high specific impulse performance of the air-breathing engine to very low thrust coefficients, making for heavy engines and engine-vehicle integration problems.
6. Higher thrust coefficients may be obtained at lower specific impulse by the injection of additional fuel and oxidizer. The highest specific impulse for propellant thrust augmentation usually is obtained with a slightly fuel-rich mixture of fuel, oxidizer, and air.

7. Propellant thrust augmentation of an air-breathing engine can provide operational flexibility, extend velocity range, and reduce variable geometry requirements but probably cannot reduce total propulsive weight as a prime operating mode.
8. Aerothermal thrust augmentation of both rocket and air-breathing powerplants is clearly profitable in cases where active cooling does not increase the airframe weight.
9. The degree of aerothermal-thrust augmentation available is subject to certain upper limits dictated by Reynolds analogy and conservation of energy, and also to lower limits if the airframe cannot survive the aerothermal environment without coolant flow.
10. A rocket-type engine capable of multimode operation as a conventional rocket, Moeckel cycle, and aerothermal rocket is an attractive combination for certain applications, giving simplicity, flexibility, and high specific impulse.

## APPENDIX A

### SUMMARY OF ANALYTIC CYCLE ANALYSIS FOR HYPERVELOCITY PROPULSION

The following is an abbreviated summary of the analytic method of cycle analysis used in this paper. It is closely parallel in form to perfect-gas-cycle analysis, to which it reduces at low flight velocity. Its chief characteristic is that it makes enthalpy and velocity the prime variables of analysis to replace the central position of temperature and Mach number in the perfect-gas formulation. All the real-gas properties essential to the analysis are contained in nozzle and inlet energy conversion parameters, which occupy the same position in the analysis as the specific heat ratio in conventional perfect-gas analysis, but which are redefined in such a way as to make the analytical formulation exact.

In principle, these energy conversion parameters should be functions of pressure level, temperature level, gas composition, nozzle-pressure ratio, inlet-pressure ratio, and all other parameters of the cycle analysis. In practice, they prove to have negligible relation to any parameters except initial enthalpy and stoichiometry. Because of this circumstance and because computed hypervelocity propulsion performance is only a weak function of the numerical value of the expansion parameter, these parameters may be picked by relatively simple correlation methods for most purposes, or even assumed constant.

To date, the method of analysis has been restricted to cycles with ideal exit nozzle expansion and single phase, chemical equilibrium flow. Under these conditions, the performance of a subsonic combustion ramjet engine is described by

$$C_F = 2\left\{\left[(1+A+E)(1+B)(1-D)\left(1-\left[\frac{C+E}{1+E}\right]^{\frac{\sigma_D(\sigma_n-1)}{\sigma_n(\sigma_D-1)}}\right)\right]^{1/2}-1\right\} \tag{1A}$$

and

$$I = \frac{C_F V}{2g\left(\frac{f+o}{a}\right)} \tag{2A}$$

Each nondimensional grouping in this equation has a physical meaning as follows:

$$A = \frac{2gJh_f}{V^2} \quad \text{nondimensionalized heat addition} \tag{3A}$$

$$B = \frac{f+o}{a} \quad \text{mass addition term} \tag{4A}$$

$$C = (1-\eta_D) \quad \text{diffuser loss term} \tag{5A}$$

$$D = (1-\eta_n) \quad \text{nozzle loss term} \tag{6A}$$

$$E = \frac{2gJh_0}{V^2} \quad \text{thermodynamic efficiency term} \tag{7A}$$

The nozzle energy conversion parameter in the exponent is formally defined as

$$\sigma_n = \left.\frac{\ln\,(P_4/P_6)}{\ln\,(P_4/P_6)-\ln\,(H_4/H_6)}\right|_S \tag{8A}$$

The inlet-energy-conversion parameter is

$$\sigma_D = \left.\frac{\ln\,(P_2/P_0)}{\ln\,(P_2/P_0)-\ln\,(h_2/h_0')}\right|_S \tag{9A}$$

Since the enthalpies are not relative but absolute values, we must choose an enthalpy zero level. In principle, the choice is arbitrary in a correlation scheme such as this. However, choice of the perfect-gas zero allows this analysis to blend smoothly into perfect-gas analysis at low enthalpies. Therefore, this choice is made. The constants given in Table 1 result.

Where high accuracy is required, values of these energy conversion parameters are picked from the correlation curve shown in Fig. 1*A* using the appropriate maximum enthalpy of the process and the appropriate equivalence ratio for air-breathers without oxidizer addition. For mixtures with substantial oxidizer addition and/or no airflow, the equivalence ratio curve is chosen having the same mole fraction of excess hydrogen. This approximation was suggested by Kushida [12]. Where the required accuracy is lower, this graphical step in the analysis may be eliminated by choosing constant values for the two energy conversion parameters more or less arbitrarily.

For convenience in handling the supersonic combustion ramjet case, we define the amount of diffusion by the additional parameter

$$\xi = \left(\frac{V_2}{V_0}\right)^2 = \text{diffuser kinetic energy ratio} \qquad (10A)$$

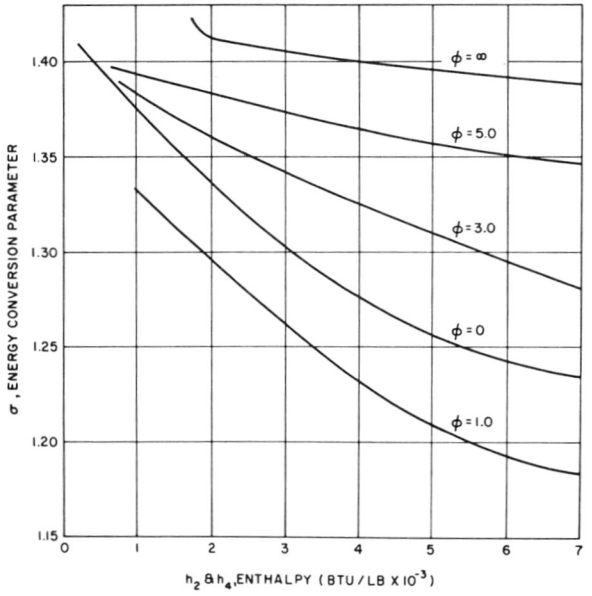


Figure 1A. Energy conversion parameter correlation.

The performance of the SCRJ engine is then

$$C_F = 2\left[\left\{(1+A+E)(1+B)(1-D) - (1+B)(1-D)\left[(1+A+E)\right.\right.\right.$$

$$\left.\left.\left. - \left(\frac{V_4}{V_0}\right)^2(1+B)\right]\left[\frac{E+C}{1-\xi+E}\right]^{\frac{\sigma_D(\sigma_n-1)}{\sigma_n(\sigma_D-1)}}\right\}^{1/2} - 1\right] \tag{11A}$$

If supersonic combustion is to be worthwhile the diffuser and nozzle loss parameters $C$ and $D$ are no longer constants but functions of $\xi$. In this analysis the relationship assumed is

$$C = (1 - \xi)C_0 \tag{12A}$$

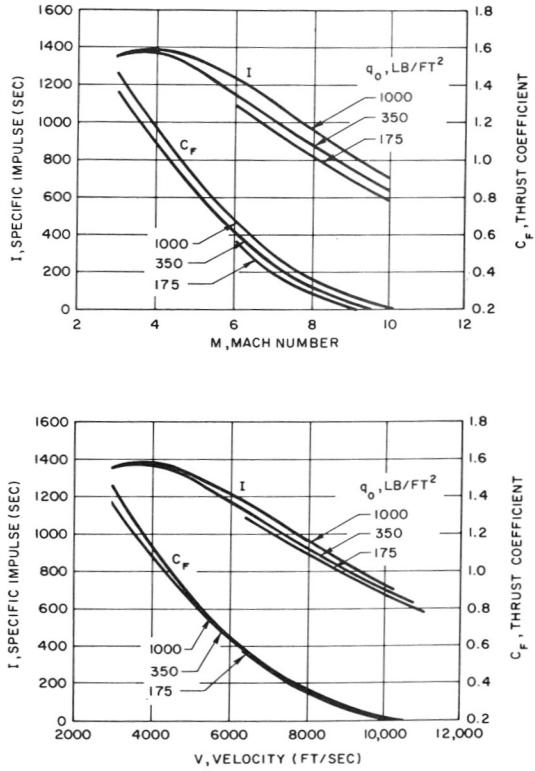


Figure 2A. Effect of choice of parameters.

and

$$D = (1 - \xi)D_0 \tag{13A}$$

where $C_0$ and $D_0$ are constants. This amounts to assuming a fixed thermodynamic process kinetic energy efficiency for the expansion and diffusion processes.

Since the fuel injection velocity is significant in the performance of the supersonic ramjet engine, we will define the parameter

$$Y = \frac{V_f}{V_0} \tag{14A}$$

If we now assume that the mixing and combustion occur at constant pressure and the fuel injection is downstream, we eliminate the velocity ratio from the equation and obtain

$$C_f = 2\left[\left\{(1 + A + E)(1 + B)(1 - D) - (1 + B)(1 - D)\right\}\left[(1 + A + E)\right.\right.$$

$$\left.\left. - \xi \frac{(1 + BY\xi^{-1/2})^2}{(1 + B)}\right]\left[\frac{C + E}{1 - \xi + E}\right]^{\frac{\sigma_D(\sigma_n - 1)}{\sigma_n(\sigma_D - 1)}}\right\}^{1/2} - 1\Bigg] \tag{15A}$$

Under the restrictions that $\sigma_D \equiv \sigma_n$, and assuming the terms of Eqs. (3A) and (7A) small compared to unity, a perturbation treatment extracts first- and second-order terms as follows:

$$C_F = (A + B - C - D) - \frac{1}{4}(A^2 + B^2 + C^2 + D^2)$$

$$+ \frac{1}{2}(AB - AC - AD - BC - BD + CD - 2AE)$$

$$- \frac{\xi}{1 - \xi}(C + E)[A + B(1 - 2Y\xi^{-1/2})] \tag{16A}$$

This relation is useful in understanding the approximate effect of the various items.

In partial justification of the choice of velocity rather than Mach number as the prime variable in hypervelocity engine performance, consider Fig. 2A, where Fig. 2 of Dugger's Ref. 2 is first reproduced and then converted to an equivalent velocity plot. The subsonic combustion performance curves for various altitudes are brought together within less than the width of the lines of the original over most of their lengths, showing

that altitude is a much weaker parameter than it appeared. This representation also points up the fact that at a velocity of 3000 fps, the two curves have the same impulse at different thrust coefficients, suggesting a minor discrepancy. Similar reduction of the apparent altitude effect is obtained by replotting supersonic combustion ramjet performance curves such as those of Ref. 1.

## SYMBOLS

| *Symbol* | *Description* | *Units* |
|---|---|---|
| $C_F$ | engine thrust coefficient | |
| $C_0$ | inlet-loss factor (see Appendix, Eq. 12) | |
| $D$ | vehicle drag | lb |
| $D_0$ | exit-loss factor (see Appendix, Eq. 13) | |
| $f/a$ | fuel-air ratio | |
| $f/o$ | fuel-oxidizer ratio | |
| $(f + o)/a$ | propellant-air ratio | |
| $g$ | gravitational constant | ft/sec$^2$ |
| $h$ | static enthalpy | Btu/lb |
| $h_f$ | propellant (fuel) heating value | Btu/lb |
| $h_0'$ | diffuser isentropic reexpansion enthalpy | Btu/lb |
| $I$ | fuel or propellant specific impulse | sec |
| $J$ | Joule's constant | ft-lb/Btu |
| $k$ | engine thrust-weight factor | lb/lb thrust |
| $P$ | pressure | lb/ft$^2$ |
| $Q$ | propellant aerothermal heat | Btu/lb |
| $R$ | friction-heat-absorption fraction | |
| $T$ | engine thrust | lb |
| $V$ | velocity | ft/sec |
| $W$ | weight | lb |
| $\dot{w}$ | fuel-weight flow rate | lb/sec |
| $Y$ | fuel-injection velocity ratio | |
| $\Delta$ | increment of | |
| $\eta_D$ | diffuser kinetic energy efficiency | |
| $\eta_n$ | nozzle kinetic energy efficiency | |
| $\eta_{th}$ | thermodynamic cycle efficiency | |
| $\eta_R$ | Moeckel cycle energy efficiency | |
| $\eta_\Delta$ | aerothermal energy conversion efficiency | |
| $\eta_\Sigma$ | overall efficiency | |
| $\nu$ | frictional-drag fraction | |
| $\xi$ | diffuser kinetic-energy ratio | |

| | |
|---|---|
| $\sigma$ | energy conversion parameter (see Appendix) |
| $\phi$ | fuel equivalence ratio |
| $\psi$ | oxidizer equivalence ratio |
| $\omega$ | thrust-drag ratio |

*Subscripts* *Stations*

| | |
|---|---|
| $a$ | aerothermal, air |
| $D$ | diffuser |
| $e$ | engine |
| $f$ | fuel, friction |
| $i$ | ideal |
| $n$ | nozzle |
| $o$ | unaugmented condition, full diffusion limit, initial |
| ox | oxidizer |
| $s$ | constant entropy |
| $st$ | stoichiometric |
| $v$ | vehicular |

*Superscripts*

| | |
|---|---|
| * | coolant enthalpy limit, Reynolds analogy limit, stoichiometry limit |

## ACKNOWLEDGMENTS

The author would like to express his appreciation to Mrs. Alice G. Taylor for the computation and plotting of the performance curves presented in this paper. For aid and constructive criticism in the earlier development of the cycle analysis methods, the author is indebted to Mr. Fred Falconer, Dr. Raymond Kushida, the late Dr. Frank Billet, and others.

## REFERENCES

1. Mordell, D. L., and J. Swithenbank, "Hypersonic Ramjets," ICAS-4, Zurich, Switzerland (September 1960).
2. Dugger, G. L., "Comparison of Hypersonic Ramjet Engines with Subsonic and Supersonic Combustion," AGARD, Milan (April 1960).
3. Ferri, A., "Possible Directions of Future Research in Air-Breathing Engines," AGARD, Milan (April 1960).
4. Drake, J. A., "Hypersonic Ramjet Development," AGARD, Milan (April 1960).
5. Weber, R. J., and J. S. MacKay, "An Analysis of Ramjet Engines Using Supersonic Combustion," NACA TN 4386 (September 1958).

6. Simkin, D., and G. C. Szego (eds.), *Elements of Space Propulsion*, New York: Wiley, (0000).
7. Moeckel, W. E., "Use of Aerodynamic Heating to Provide Thrust by Vaporization of Surface Coolants," NACA TN 3140 (1954).
8. Greiner, L., I. Micholson, and J. Rubenowitz, "Hypersonic Flight without Overheating: I. Friction Heat Absorption and Thrust Gain by Use of Coolant Fuels," AFOSR TN-57-374, Ordin Associates, Pasadena, California (June 1957).
9. Gordon, S., and B. J. McBride, "Theoretical Performance of Liquid Hydrogen with Liquid Oxygen as a Rocket Propellant," NASA Memo 5-21-59E (June 1959).
10. Eggers, A. J., Jr., and H. J. Allen, "A Comparative Analysis of the Performance of Long-Range Hypervelocity Vehicles," NACA TN 4046 (October 1957).
11. Dukes, W. H., "Protection of Aircraft Structures against High Temperatures," ICAS-4, Zurich, Switzerland (September 1960).
12. Kushida, Raymond, private communication.